ECS Transactions, 58 (8) 87-92 (2013)
10.1149/05808.0087ecst ©The Electrochemical Society

Spatially Resolved Optoelectronics in Lead Sulfide Nanowires

Yiming Yang, Xingyue Peng, and Dong Yu

Department of Physics, University of California, Davis, CA 95616, USA

Spatially resolved optoelectronic investigation can reveal important information on charge transport and recombination in field-effect transistors (FETs) incorporating single nanowires (NWs). Scanning photocurrent microscopy (SPCM) was performed on single PbS NW FETs to extract diffusion length and lifetime of minority carriers as a function of gate voltage and excitation intensity. Interestingly, we observed a reverse of the photocurrent direction in gate-depleted PbS NW FETs under high intensity illumination. We attribute this effect to the back-gate induced carrier concentration gradient.

Introduction

Lead sulfide (PbS) nanostructures, such as nanowires (NWs) and quantum dots (QDs), have attracted intensive attention due to their promising applications in photovoltaic devices.[1~4] With a direct bandgap of 0.41 eV at room temperature, PbS possesses many properties favorable to the fabrication of optoelectronic devices, such as high absorption coefficient, high carrier mobility, and long carrier lifetime. Recently, our group demonstrated a chemical vapor deposition (CVD) technique of synthesis and ambipolar doping of PbS NWs. [5] By varying the growth condition, we were able to tune the carrier concentration in a large range, from 8×10^{18} cm^{-3} (p-type) to 10×10^{18} cm^{-3} (n-type). Optoelectronic measurements of PbS single NW FETs were performed on our home-build scanning photocurrent microscope (SPCM) platform. As a focused laser is scanned along the NW, photo carriers (electrons and holes) are locally injected into the NW. Subsequently, photocurrent is measured by collecting the photo-carriers through an external circuit. By using SPCM, we have measured minority carrier diffusion lengths, an important optoelectronic parameter, in PbS NWs as a function of gate voltage. As the gate depletes the carriers in the NWs, the lifetime is increased by orders of magnitude. [5]

In this paper, we focus on how photocurrent depends on excitation intensity. At high intensity, the photocurrent does not simply increase linearly with the intensity. We found that even the photocurrent direction could reverse at the high-level injection. Understanding the behavior of photogenerated carriers in semiconductors is essential to the development and optimization of optoelectronic devices such as solar cells and photodetectors. Comparing to the semiconductor's dark carrier concentration, the photo-carrier injection level can be classified into low, moderate and high injection regimes depending on the illumination intensity. Particularly, in the high-level injection regime where the photo-injected carrier concentration is higher than that in the dark, the redistribution of electric field in the semiconductors can lead to electronic properties drastically different from the low-level injection. The high-level regime is met in many applications such as concentrated solar energy devices and lasers. Therefore, it is

Downloaded on 2016-09-16 to IP 130.203.136.75 address. Redistribution subject to ECS terms of use (see ecsdl.org/site/terms_use) unless CC License in place (see abstract).

important to investigate and understand the optoelectronic properties of semiconductor devices at high excitation intensity. Here, we report a current reverse phenomenon observed in PbS NWs FETs under high intensity. We believe the back gate-induced electric field along the NW is responsible for the current flipping.

Experimental Details

Synthesis and Device Fabrication

PbS NWs were synthesized by a CVD method in a tube furnace. $PbCl_2$ (99.999%, Alfa Aesar) and S (99.9999%, Alfa Aesar) powders were used as the precursors of the synthesis. 200 nm Ti thin films coated on the Si substrates were used as a catalyst for the NW growth. Doping PbS NWs was realized by varying the mass ratio of the $PbCl_2$ and S powders. Other details of the growth can be found in our previous work. [5] The as-grown NWs were transferred onto 300 nm SiO_2 covered, highly doped p-type Si substrates. Subsequently, electrical contacts (75nm Au/75nm Cr) were defined using electron beam lithography followed by lift-off.

Optoelectronic Characterization

Current-voltage (*I–V*) curves were measured through a current preamplifier (DL Instruments, model 1211) and a NI data acquisition system. Optoelectronic measurement was performed on our scanning photocurrent microscopy (SPCM) platform. Detailed description of our SPCM setup can be found elsewhere. [5] Briefly, a 532 nm CW laser was focused by a 100× N.A. 0.95 objective lens to a Gaussian beam with full width at half maximum (FWHM) of 430 nm and raster scanned on a planar device by a pair of mirrors mounted on a galvanometer, while both the reflection and the photocurrent were simultaneously recorded to produce a 2-dimensional map of photocurrent. The intensity of the laser was controlled by a set of neutral density (ND) filters and the laser power was measured by a power meter (Thorlabs).

Results and Discussion

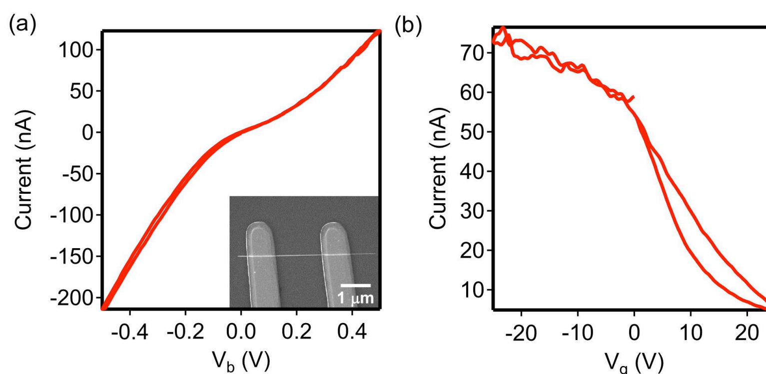

Figure 1. Electrical characteristics of PbS NW FETs. (a) I–V_b curves for a p-type PbS NW. Inset: SEM image of a typical PbS single NW FET. (b) Current at V_b = 0.3 V as V_g sweeps at a rate of 2.5 V/s.

Downloaded on 2016-09-16 to IP 130.203.136.75 address. Redistribution subject to ECS terms of use (see ecsdl.org/site/terms_use) unless CC License in place (see abstract).

Dark I-V characteristics of a PbS NW FET are shown in Figure 1(a). The SEM image of a typical device is shown in the inset. The PbS NW in the measured device is 12 μm long between two metal contacts, with a diameter of 108 nm. The slight nonlinearity of I-V curve is likely due to the asymmetry of the two contact junctions created in the fabrication process. By applying a gate voltage (V_g), we are capable of extracting the mobility and concentration of the majority carrier. P-type carrier behavior is observed in the gate sweep (Figure 2(b)), with mobility of 18 cm^2/Vs and carrier concentration of 8 x 10^{17} cm^{-3} for holes. The mobility for holes is consistent with our previous report. [5]

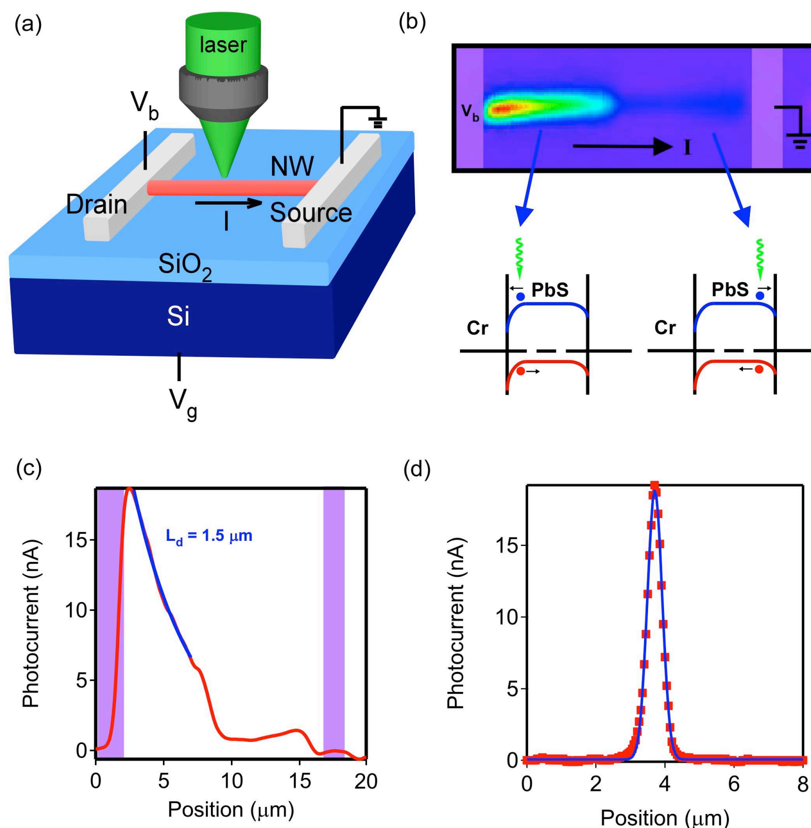

Figure 2. (a) Schematic diagram of SPCM setup. (b) SPCM image at $V_g = V_b = 0$ V of a p-type PbS NW FET. Purple regions indicate the position of contacts. Laser power is 1 μW at 532 nm. (c) Photocurrent line-scan along the NW. The blue curve is the exponential fitting to extract the photocurrent decay length. The shaded areas indicate the contacts. (d) Photocurrent line-scan perpendicular to the NW. The blue curve is the Gauss fitting to determine the FWHM of the laser spot. FWHM of 430 nm is obtained from the fitting.

In order to investigate the optoelectronic properties of the device, we carry out SPCM measurements (data shown in Figure 2 (b)). The direction of the photocurrent is consistent with a band bending downward towards the Cr contact. The detailed description of band bending diagrams can be found elsewhere. [6] The photocurrent near the right contact is much smaller in magnitude, indicating a nearly ohmic contact. The asymmetry of the two contacts is likely caused by the slight difference of the two contacts in the fabrication process as reported before. [5] Figure 2 (c) shows a line-scan along the NW axis. The photocurrent curve near the left contact can be fitted nicely with an exponential function, which allows us to extract the minority carrier diffusion length,

Downloaded on 2016-09-16 to IP 130.203.136.75 address. Redistribution subject to ECS terms of use (see ecsdl.org/site/terms_use) unless CC License in place (see abstract).

$l_D = \sqrt{D\tau}$, where $D = \mu k_B T / q$ is the minority carrier (electron) diffusion coefficient, μ is the minority carrier mobility, q is electron charge, k_B is Boltzman constant, T is temperature, and τ is the minority carrier lifetime. The minority carrier diffusion of 1.5 μm is obtained from the fitting for this device. Figure 2 (d) demonstrates a line-scan perpendicular to the NW, which can be fitted with a Gaussian function, with a full width at half maximum (FWHM) of 430 nm, in agreement with the focused laser spot size.

We will first show the gate dependent SPCM results at low intensity. As shown in Figure 3, both the photocurrent direction and magnitude strongly depend on V_g, as the band bending is a function of V_g, which can significantly modulate photocurrent. At V_g = 0 V, the positive photocurrent on the left side is corresponding to a downward band bending towards Cr. At V_g = -50 V, the band bending increases, leading to a more efficient charge separation and a higher photocurrent. At V_g = +50 V, the band bending is flipped, resulting in a reversed photocurrent.

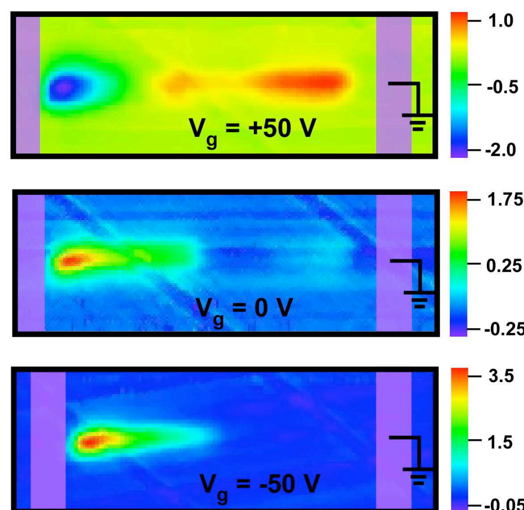

Figure 3. SPCM images at V_b = 0 V and V_g = +50 V, 0 V and -50 V, respectively, from top to bottom. The laser power is 100 nW. The unit of color scale on the right is in nA. The shaded areas indicate the contacts.

Interestingly, at V_g = 50 V where the band is nearly flat, the direction of the photocurrent can be reversed in this PbS NW FET as excitation intensity is increased. As shown in Figure 4 (a), at low intensity, the photocurrent near the left contact is negative, indicating the band bends upward towards contact. At high intensity, the photocurrent image shows a complex feature near the left contact. When the laser spot is right on top of the NW near the left contact, the photocurrent is positive, opposite to the direction at low intensity. On the contrary, the photocurrent remains negative as the laser spot is off centered, giving two negative wings to the positive central spot. To better examine this interesting phenomenon, we show the cross section of the SPCM image perpendicular to the NW near the left contact in Figure 4 (b). At low intensity, the photocurrent profile follows a simple Gaussian distribution while at higher intensity it shows a more complicated "W"-shaped curve, with a positive photocurrent at the center and two negative dips near the central peak. This photocurrent profile is reproducible and robust, independent of scan direction and scan speed, and has been also seen in several other devices. At gate voltage

Downloaded on 2016-09-16 to IP 130.203.136.75 address. Redistribution subject to ECS terms of use (see ecsdl.org/site/terms_use) unless CC License in place (see abstract).

where the band bending is large ($V_g < 20$ V or $V_g > 50$ V), the photocurrent direction remains the same at all intensities tested (positive at $V_g < 20$ V and negative at $V_g > 50$ V at the left contact).

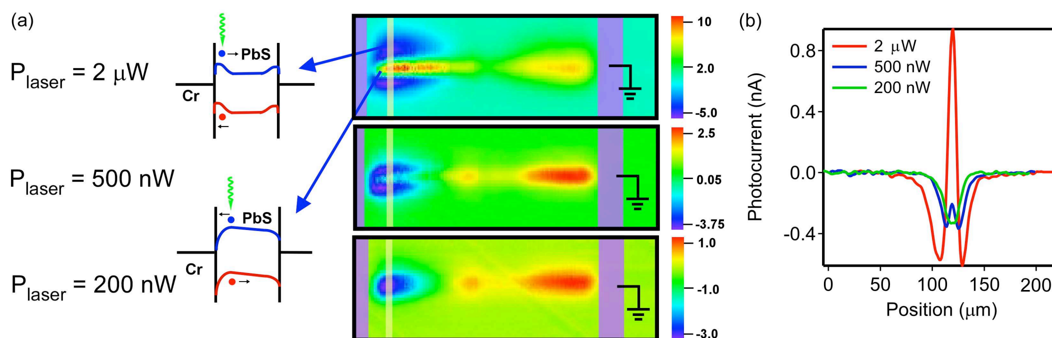

Figure 4. (a) SPCM image at $V_b = 0$ V, $V_g = +50$ V and $P_{laser} = 2$ µW, 500 nW and 200 nW, respectively, from top to bottom. The unit of color scale on the right is in nA. The shaded areas indicate the contacts. (b) Photocurrent line-scans perpendicular to the NW near the left contact, taken at the position indicated by the yellow vertical lines in (a).

This "W" shape can be understood by considering the Gaussian distribution of the laser spot. When the laser is centered a few hundred nanometers away from the NW, the NW is exposed to the tail of the Gaussian beam and thus the actual excitation intensity on the NW is significantly decreased. Therefore, the wings in the SPCM image correspond to the photocurrent at low intensity. This explanation is further supported by the low intensity scan as in the bottom image of Figure 4 (a). What remains to be understood is why the photocurrent is negative at low intensity and positive at high intensity near the left contact.

We attribute the intensity dependent photocurrent direction to the non-uniform gating efficiency in the NW FET. As a gate voltage is applied to the NW FET, the gate-induced electric field is partially screened near the metal electrodes, leading to a less efficient gate effect near the contact. Therefore, while the holes in the central NW segment away from the contacts are repelled by the applied positive gate voltage, the hole concentration remains high near the contacts. The difference in the hole concentrations results in an internal electric field which drives the negative photocurrent at the left contact under the low-level injection (band bending diagram at low intensity is shown at the top of Figure 4(a)). At higher intensity, the injected carrier concentration is higher than the dark carrier concentration, thus mitigating the gate induced carrier concentration gradient (band bending diagram at high intensity is shown at the bottom of Figure 4(a)). In this case, the band bending at the contacts dictates the photocurrent direction, leading to a reversed current. We have carried out numerical modeling which supports this explanation. More experiment and theoretical study is needed to further investigate this effect.

Conclusions

In summary, we have studied local band bending and charge transport and recombination in single PbS NW FETs by using a spatially resolved optoelectronic technique. SPCM reveals that photocurrent is reversed in a gate-depleted PbS NW under high intensity illumination. The gate-induced carrier concentration gradient due to the contact screening

Downloaded on 2016-09-16 to IP 130.203.136.75 address. Redistribution subject to ECS terms of use (see ecsdl.org/site/terms_use) unless CC License in place (see abstract).

likely accounts for such a phenomenon. At high excitation intensity, the injected carriers can reduce such a gradient and lead to a reverse in current. Our experimental data provide useful information to optoelectronic systems and devices under high carrier injection such as lasers and concentrated solar power (CSP). CSP is widely used in solar cell systems due to its advantages of gaining the power conversion efficiency and reducing the cell cost. Typically, 1000~10000 sun intensity is achieved in CSP. Our results suggest that these nonlinear effects need to be considered in device design and fabrication.

Acknowledgments

This work was supported by the U.S. National Science Foundation Grant DMR-1310678. Work at the Molecular Foundry was supported by the Office of Science, Office of Basic Energy Sciences, of the U.S. Department of Energy under Contract No. DE-AC02-05CH11231.

References

1. McDonald, S. A.; Konstantatos, G.; Zhang, S. G.; Cyr, P. W.; Klem, E. J. D.; Levina, L.; Sargent, E. H. *Nat. Mater,* **4**, 138 (2005).
2. Schaller, R. D.; Klimov, V. I. *Phys. Rev. Let,* **92**, 186601 (2004).
3. Ellingson, R. J.; Beard, M. C.; Johnson, J. C.; Yu, P. R.; Micic, O. I.; Nozik, A. J.; Shabaev, A.; Efros, A. L. *Nano Lett,* **5**, 865 (2005).
4. Wu, H. K.; Yang, Y. M.; Oh, E.; Lai, F. C.; Yu, D. *Nanotechnology,* **23**, 265602 (2012).
5. Yang, Y.; Li, J.; Oh, E.; Yu, D. *Nano Lett,* **12**, 5890 (2012).
6. Graham, R.; Miller, C.; Oh, E.; Yu, D. *Nano Lett,* **11**, 717 (2011).

Downloaded on 2016-09-16 to IP 130.203.136.75 address. Redistribution subject to ECS terms of use (see ecsdl.org/site/terms_use) unless CC License in place (see abstract).